Quantum search at low temperature in the single avoided crossing model

Parth Ashvinkumar Patel

A Thesis presented for the degree of
Master of Science by Research

Dr. Vivien Kendon
Department of Physics
University of Durham
England

August 2019

Dedicated to

My parents for supporting me throughout my studies.

Quantum search at low temperature in the single avoided crossing model

Parth Ashvinkumar Patel

Submitted for the degree of Master of Science by Research
August 2019

Abstract

We begin with an n-qubit quantum search algorithm and formulate it in terms of quantum walk and adiabatic quantum computation. We then represent and transform the n-qubit search algorithm into a two-level system and hence the single avoided crossing model. We perform and present the analytical calculations and numerical simulations of the dynamics of quantum walk search algorithm and AQC search algorithm in a thermal bath. We use the master equations formulation to represent the open quantum system. We find out that while generally the performance of algorithms worsen with increase in temperature and the system size, there are interesting features in quantum walk search where there is an optimal low temperature for the best performance for other specified parameters. Similarly for AQC search, the performance generally worsens with increase in temperature, but for specified parameter ranges, the system is more robust against temperature effects.

Declaration

Acknowledgements

I would like to thank my project supervisor, Dr. Vivien Kendon and co-supervisor Dr. Nicholas Chancellor, who guided and supported me throughout this project. I would also like to thank Prof. Simon Gardiner who helped me clear my doubts about some of the mathematical formulations. I also want to thank my colleagues for the helpful discussions.

Contents

Abstract **iii**

Declaration **iv**

Acknowledgements **v**

1 Introduction **1**

2 Background **4**

2.1 Quantum walk 4

2.2 Adiabatic quantum computation 6

2.3 Quantum search problem 8

2.3.1 Quantum walk search 8

2.3.2 Adiabatic quantum computation search 11

2.4 Single avoided crossing model 13

2.5 Open quantum system 15

3 Open quantum system for quantum walk search **18**

3.1 Analytics 18

3.2 Numerical Analysis 22

4 Open quantum system for adiabatic quantum computation **29**

4.1 Analytics 29

4.2 Simulations 33

5 Conclusions **40**

Bibliography **43**

Appendix **47**

A Analytical expansion of Lamb shift terms for QW search **47**

B Components of density matrix in solution of AQC search **48**

List of Figures

3.1 Plotting probability, P of being in ground state of quantum walk search Hamiltonian in computational basis in an ohmic bath while varying coupling strength, g^2 vs runtime, t for specified values of inverse temperature, β and minimum energy gap, g_{min}. The single avoided crossing model describing a two-level approximation of multi-qubit quantum walk search in presence of an ohmic bath is being analysed. The plots provide an outlook on the valid ranges of coupling strength under different values of the parameters. 23

3.2 Plotting probability, P of being in ground state of quantum walk search Hamiltonian in computational basis in an ohmic bath while varying inverse temperature, β vs runtime, t for specified values of coupling strength, g^2 and minimum energy gap, g_{min}. The single avoided crossing model describing a two-level approximation of multi-qubit quantum walk search in presence of an ohmic bath is being analysed. The plots provide an outlook on the performance of search algorithm at different temperatures for specified values of other parameters. 24

3.3 Plotting cost factor, T while varying coupling strength, g^2 vs inverse temperature, β for the first peak of probability, P of being in ground state of quantum search Hamiltonian in computational basis and specified minimum energy gap, g_{min} to describe how worse off the search algorithm is performing in the presence of an ohmic bath, compared to the best theoretical time to get the solution predicted by the two-level approximation in absence of the bath. The 2-d slice plots (d) and (e) provide a clearer picture of the cost factor variation at different values of the parameters. The single avoided crossing model describing a two-level approximation of multi-qubit quantum walk search in presence of an ohmic bath is being analysed. 25

3.4 Plotting cost factor, T while varying inverse temperature, β vs number of basis states, N for the first peak of probability, P of being in ground state of quantum search Hamiltonian in computational basis for specified values of coupling strength, g^2 to describe how worse off the search algorithm is performing in the presence of an ohmic bath, compared to the best theoretical time to get the solution predicted by the two-level approximation in absence of the bath. Note the colour scales for T are different in each sub-figure. The 2-d slice plots (d) and (e) provide a clearer picture of the cost factor variation at different values of the parameters. The single avoided crossing model describing a two-level approximation of multi-qubit quantum walk search in presence of an ohmic bath is being analysed. 27

4.1 Plotting probability, $P(t_f)$ of being in instantaneous ground state of the AQC search Hamiltonian in computational basis while varying coupling strength, g^2 vs final runtime, t_f for specified values of inverse temperature, β and minimum energy gap, g_{min}. The 2-d slice plots (d) and (e) provide a clearer picture of the variation of $P(t_f)$ at different values of the parameters. The single avoided crossing model describing a two-level approximation of multi-qubit AQC search in presence of an ohmic bath is being analysed. The plots provide an outlook on the valid ranges of coupling strength under different values of other parameters and show that having longer runtimes to achieve higher success probability may not be suitable in the presence of an ohmic bath. 35

4.2 Plotting probability, $P(t_f)$ of being in instantaneous ground state of the AQC search Hamiltonian in computational basis while varying inverse temperature, β vs final runtime, t_f for specified values of coupling strength, g^2 and minimum energy gap, g_{min}. Note the colour scales for T are different in each sub-figure. The 2-d slice plots (d) and (e) provide a clearer picture of the variation of $P(t_f)$ at different values of the parameters. The single avoided crossing model describing a two-level approximation of multi-qubit AQC search in presence of an ohmic bath is being analysed. The plots provide an outlook on the variation of $P(t_f)$ with temperature under specified values of other parameters. 37

4.3 Plotting probability, $P(t_f)$ of being in instantaneous ground state of AQC search Hamiltonian in computational basis while varying minimum energy gap, g_{min} vs inverse temperature, β for specified values of coupling strength, g^2 and final runtime, t_f. Note the colour scales for P are different in each sub-figure. The 2-d slice plots (d) and (e) provide a clearer picture of the variation of $P(t_f)$ at different values of the parameters. The single avoided crossing model describing a two-level approximation of multi-qubit AQC search in presence of an ohmic bath is being analysed. The plots provide an outlook on the variation of $P(t_f)$ under different temperatures and system sizes with specified values of other parameters. They show that under specific operating ranges of parameters, the values of $P(t_f)$ is more robust under temperature effects. 39

Chapter 1

Introduction

With the decline of Moore's law and the advent of quantum supremacy, a lot of research is being to done to make use of quantum effects to build quantum computers which provide speedup over the current classical limits. To make use of quantum computers, we need quantum algorithms to run and support their functionality. While the standard gate model quantum computing has been very popular to this effect, in the past two decades a lot of research has also been done in continuous time quantum computing, leading to the development of quantum walk [1] [2], quantum annealing [3] and adiabatic quantum computation(AQC) [4] formulations.

The structure of mathematical formulation describing quantum annealing and AQC is the same. However, depending on the instantaneous speed of change over time of the Hamiltonian, quantum annealing can have two forms: adiabatic computation (very slow speed) or diabatic computation. AQC describes a class of quantum computation where instantaneous speed of change over time of the Hamiltonian is very slow. While quantum annealing has the added requirement that the initial state is an equal superposition of all possible basis states, AQC has no such requirement.

Quantum walks, quantum annealing and AQC have contributed a lot for the

development of an alternative representation of gate model quantum algorithms [5] [6] [7] suitable for real world applications e.g., searching unsorted databases, optimization problems, sampling problems, etc. However, we have been limited in our quest to build true quantum computers, due to the quantum effects being easily decohered by noise due to the environment, in spite of applying quantum error correction codes [8] [9] [10]. For this work, we are going to focus on quantum walk and AQC.

Open quantum system formulation plays a major role in describing the performance of quantum systems in real world dynamics. One of the key factors in real world dynamics is the effects on the system due to the temperature of the environment the system is working in. Although we aim to build systems where system is highly isolated from such disturbances, but for realistic systems we are always affected with a certain amount of noise. Some of the noise is generated by the engineering components of system itself and is unavoidable.

In chapter 2, we provide an outline of what quantum walk and adiabatic quantum computation entails. Then, we give a brief introduction about how they are used to solve the quantum search problem. We also provide background details about the single avoided crossing model which allows us to simplify our model for a large number of qubits to a two-level system. Then we provide the outline of the open quantum system formulation we will be using to describe our problem.

In chapter 3, we solve analytically the performance for quantum walk algorithm for solving the quantum search problem in the single avoided crossing model setting in presence of temperature effects. With varying coupling strengths of the quantum system with the environment, we observe the different finite temperature effects in the weak coupling limit and the quasi-intermediate coupling regime. We also plot the numerical simulations to give us a better understanding of the performance of the quantum walk.

In chapter 4, we solve analytically the performance for adiabatic quantum computation algorithm for solving the quantum search problem in the single avoided crossing model setting in presence of temperature effects. With varying coupling strengths of the quantum system with the environment, we observe the different finite temperature effects in the weak coupling limit and the quasi-intermediate coupling regime. We plot the numerical simulations to give us a better understanding of the performance of the adiabatic quantum computation.

In chapter 5, we conclude our observations and analysis. While generally the performance of algorithms worsen with increase in temperature and the system size for both quantum walk and AQC, there are interesting features to be explored like the existence of optimal temperature in quantum walk and increased robustness against temperature in AQC for certain parameter ranges.

Chapter 2

Background

In this chapter we provide the detailed information about the theoretical ideas and formulation we use to describe our problem and the tools we use to solve it.

2.1 Quantum walk

While there are two basic types of quantum walks- discrete and continuous time [2], we focus our work on the continuous time quantum walks. Continuous-time quantum walks on a discrete lattice have their origins back as far as Feynman et al. [11]. Their use for quantum algorithms was first suggested by Farhi and Gutmann [12], who showed numerically they can reach the ends of certain network configurations more efficiently than classical random walks. A proven exponential speed up in a quantum algorithm using a continuous-time quantum walk came a few years later from Childs et al. [13]. Our motivation to use quantum walks comes from the fact that quantum walks have been shown to be universal in defining algorithms for quantum computation [14].

A continuous-time quantum walk can be defined by considering the labels j of

the n-qubit basis states $\{|j\rangle\}$ to be the labels of vertices of an undirected graph G. The edges of G can be defined through its adjacency matrix A, whose elements satisfy $A_{jk} = 1$ if an edge in G connects vertices j and k and $A_{jk} = 0$ otherwise. Since G is undirected, A is symmetric, hence it can be used to define a Hamiltonian. Although we can use the adjacency matrix A directly, it is in general more convenient mathematically to define the Hamiltonian of the quantum walk using the Laplacian $L = D - A$, where D is a diagonal matrix with entries $D_{jj} = d_j$ the degree of vertex j in the graph. We follow this convention here, but note that in this work we use regular graphs for which the degree $d_j = d$ is the same for all vertices, so that $D = d\mathbb{1}$, where $\mathbb{1}$ is the identity matrix (ones on the diagonal) of the same dimension as A. Terms proportional to the identity in the Hamiltonian shift the zero point of the energy scale and contribute an unobservable global phase, but otherwise don't affect the dynamics. The quantum walk Hamiltonian is then defined as $\hat{H}_{QW} = \gamma\hat{L}$, where $\hat{L}$ is the Laplacian operator, and the prefactor γ is the hopping rate of the quantum walk. For any regular graph of degree d we thus have

$$\hat{H}_{QW} = \gamma\left(d\hat{\mathbb{1}} - \sum_{jk} A_{jk} |j\rangle \langle k|\right) \equiv \gamma(d\hat{\mathbb{1}} - \hat{A}), \tag{2.1}$$

where the adjacency operator $\hat{A}$ has matrix elements in the vertex basis $\{|j\rangle\}$ given by the adjacency matrix A. The action of $\hat{H}_{QW}$ is to move amplitude between connected vertices, as specified by the non-zero entries in A. During a quantum walk, a pure state $|\psi(0)\rangle$ evolves according to the Schrödinger equation to give

$$|\psi(t)\rangle = e^{-i\hat{H}_{QW}t} |\psi(0)\rangle \tag{2.2}$$

after a time t, where we have used the units in which $\hbar = 1$.

The pure state evolution of the continuous-time quantum walk can be expressed

in density matrix form as

$$\frac{d\rho(t)}{dt} = -i[\hat{H}_{QW}, \rho], \tag{2.3}$$

where $[a, b] \equiv ab - ba$ denotes the commutator. Using open quantum system dynamics, we can add a non-unitary decoherence to this in the form

$$\frac{d\rho(t)}{dt} = -i[\hat{H}_{QW}, \rho] + \mathcal{L}[\rho(t)], \tag{2.4}$$

where $\mathcal{L}$ is the superoperator describing the effective decoherence dynamics. Elaborate description of $\mathcal{L}$ been provided in section 2.5 .

2.2 Adiabatic quantum computation

Adiabatic quantum computation (AQC), first introduced by Farhi et al. [4], works as follows. The problem of interest is encoded into an n-qubit Hamiltonian $\hat{H}_p$ in such a way that the solution can be derived from the ground state of $\hat{H}_p$. The system is initialized in the ground state of a different Hamiltonian $\hat{H}_0$, for which this initialization is easy. The computation then proceeds by implementing a time-dependent Hamiltonian that is transformed slowly from $\hat{H}_0$ to $\hat{H}_p$. In general, this adiabatic 'sweep' Hamiltonian can be parametrized in terms of a time-dependent schedule function $s(t) \in [0, 1]$ as

$$\hat{H}_{AQC}(t) = (1 - s(t))\hat{H}_0 + s(t)\hat{H}_p, \tag{2.5}$$

such that $s(t = 0) = 0$ and at the final time t_f we have $s(t = t_f) = 1$. It is useful to define a reduced time $\tau = t/t_f$, with $0 \leq \tau \leq 1$. Whereas τ is linear in t, the schedule function $s(\tau)$ - written as a function of t or τ - allows for non-linear

transformation. Non-linear schedules are essential to obtain a quantum speed up in the search problem [15], this fact has been elaborated upon in Section 2.3 and 2.4.

The adiabatic theorem of quantum mechanics [16] says that the system will stay in the instantaneous ground state of the time-dependent Hamiltonian $\hat{H}_{AQC}(t)$ provided the following two conditions are satisfied: (i) there is at all times an energy gap $g(t) > 0$ between the instantaneous ground and first excited states, and (ii) the Hamiltonian is changed sufficiently slowly. Provided these are both true the system will be in the desired ground state of $\hat{H}_p$ at the end of the computation, thus solving the problem encoded in $\hat{H}_p$. In practice, the duration of this adiabatic sweep would be prohibitively long, so a feasible sweep will incur some probability of error. The runtime for the algorithm can be bounded by

$$T_{runtime} = O\Big(\frac{1}{g_{min}^2}\Big), \tag{2.6}$$

where g_{min} is the minimum spectral gap of $\hat{H}_{AQC}(s)$.

AQC is a possible method to get around the problem of energy relaxation. Since the quantum system is in the ground state, interference with the outside world cannot make it move to a lower state. If the energy of the outside world (i.e., the "temperature of the bath") is kept lower than the energy gap between the ground state and the next higher energy state, the system has a proportionally lower probability of going to a higher energy state. Thus the system can stay in a single system eigenstate as long as needed. For a comprehensive overview of AQC, see Albash and Lidar [17]. Adiabatic quantum computation has been shown to be equivalent to the standard quantum computation [18].

2.3 Quantum search problem

The quantum search problem, first introduced by Grover [19] can be framed in terms of the $N = 2^n$ basis states of an n-qubit system $\{|j\rangle\} = \{|0\rangle, |1\rangle\}^{\otimes n}$, where $\{|0\rangle, |1\rangle\}$ is the basis of a single qubit. We are given that one of the basis states behaves differently to the others and denote this 'marked' state as $|m\rangle$, where m is an n-digit bit-string identifying one of the basis states. Because of the difference in behaviour, we can easily verify whether a given state is the marked state. We represent an ignorance of the marked state by starting with the system in a uniform superposition over the basis states,

$$|\psi_{init}\rangle = \frac{1}{\sqrt{N}} \sum_{j=0}^{N-1} |j\rangle . \tag{2.7}$$

2.3.1 Quantum walk search

Quantum walk dynamics can be used to solve the search problem by modifying the energy of the marked state $|m\rangle$ to give a quantum walk search Hamiltonian

$$\hat{H}_{QWS} = \gamma(d\hat{\mathbb{1}} - \hat{A}) - |m\rangle \langle m| . \tag{2.8}$$

In the units we are using, this amounts to giving state $|m\rangle$ an energy of -1 while all other states have zero energy. This also makes γ a dimensionless parameter controlling the ratio of the strengths of the two parts of the quantum walk search Hamiltonian. Applying $\hat{H}_{QWS}$ to the search initial state $|\psi_{init}\rangle$ produces a periodic evolution such that the overlap with the marked state oscillates. The frequency of these oscillations depends on the hopping rate γ, which must be chosen correctly, along with the measurement time t_f to maximize the final success probability $P = |\langle\psi(t_f)|m\rangle|^2$, where $|\psi(t_f)\rangle = e^{-i\hat{H}_{QWS}t_f} |\psi_{init}\rangle$ is the state at time t_f .

The adjacency matrix of an n-dimensional hypercube graph has elements $A_{jk} = 1$ if and only if the vertex labels j and k have a Hamming distance of one. That is, when written as n-digit bit-strings, they differ in exactly one bit position. The corresponding adjacency operator can be conveniently expressed as

$$\hat{A}^{(h)} = \sum_{j=1}^{n} \hat{\sigma}_x^{(j)}, \tag{2.9}$$

where the sum is over all n qubits and $\hat{\sigma}_x^{(j)}$ is the Pauli-X operator applied to the jth qubit with the identity operator on the other qubits. That is,

$$\hat{\sigma}_x^{(j)} = \left(\bigotimes_{r=1}^{j-1} \hat{\mathbb{1}}_2 \right) \otimes \hat{\sigma}_x \otimes \left(\bigotimes_{r=j+1}^{n} \hat{\mathbb{1}}_2 \right), \tag{2.10}$$

where $\otimes$ denotes the tensor product, and $\hat{\mathbb{1}}_2$ is the identity operator of dimension two. To construct the quantum walk search Hamiltonian on the hypercube, we include two trivial adjustments for later mathematical convenience. If we make the energy of the marked state lower by adding $\hat{\mathbb{1}} - |m\rangle \langle m|$ to the quantum walk Hamiltonian, this gives the marked state an energy of zero while all other states have an energy of one for this part of the Hamiltonian. The factor of half has been included in $\hat{H}_0$ to match Refs. [20] [4] [21] and facilitate the mapping to the symmetric subspace for solving the eigensystem of the search Hamiltonian and calculation of hypercube schedules for AQC as analysed in Appendix A of [22]. The Laplacian operator for a hypercube can thus be represented as

$$\hat{H}_0 = \frac{1}{2}\Big(n\hat{\mathbb{1}} - \sum_{j=1}^{n} \hat{\sigma}_x^{(j)} \Big). \tag{2.11}$$

The problem Hamiltonian describing the marked state is

$$\hat{H}_P = \hat{\mathbb{1}} - |m\rangle \langle m| . \tag{2.12}$$

Quantum walk search Hamiltonian can thus be represented as

$$\hat{H}_{QWS} = \gamma \hat{H}_0 + \hat{H}_P. \tag{2.13}$$

The notation of $\hat{H}_0$ and $\hat{H}_P$ used for the Laplacian operator and the problem Hamiltonian describing the marked state respectively is for the convinience in further calculations during the rest of the work.

Childs and Goldstone [20] analyze the quantum walk search algorithm for both the complete and hypercube graphs. For each graph, they find optimal values of γ for which the performance of the search matches the quadratic quantum speed up achieved by Grover's search algorithm. Childs and Goldstone [20] tune γ until both the initial state $|\psi_{init}\rangle$ and the marked state $|m\rangle$ have significant overlap with both the ground state $|\varepsilon_0\rangle$ and the first excited state $|\varepsilon_1\rangle$ of the search Hamiltonian. Intuitively, we want the search Hamiltonian to drive transitions between $|\psi_{init}\rangle$ and $|m\rangle$ as efficiently as possible. This occurs when the overlaps are evenly balanced, which in turn occurs when the energy gap, $g = \varepsilon_1 - \varepsilon_0$ between the ground and first excited state is smallest: g_{min}. With this optimally chosen value of γ, the time it takes for the transition to occur turns out to be proportional to $1/g_{min}$. For the hypercube graph, optimal hopping rate γ_o is

$$\gamma_o = \frac{1}{N} \sum_{r=1}^{n} \binom{n}{r} \frac{1}{r}. \tag{2.14}$$

For the optimal γ_o, the time to reach the first maximum overlap with the marked state is

$$t_h \simeq (\pi/2)\sqrt{N} \propto (1/g_{min}), \tag{2.15}$$

providing a quadratic speed up equivalent to Grover's original search algorithm. The energy gap is analyzed in Section 4.2 of [4], and the energy eigenstates are

analyzed in Appendix B of [21]. At optimal γ_o, the ground and first excited states are $\frac{1}{\sqrt{2}}(|\psi_{init}\rangle \pm |m\rangle)$. Since states of higher energy than the first excited state play very little role in the QW search dynamics for larger systems, we can approximate the probability that the marked state can be reached by considering only the ground and first excited states, essentially a two-level system. In Section 2.4, we provide the single avoided crossing model for describing such a two-level system.

2.3.2 Adiabatic quantum computation search

In order to make a direct comparison between AQC search and QW search, the $\hat{H}_0$ and $\hat{H}_p$ are chosen to be the same. Thus,

$$\hat{H}_{AQC} = \frac{1}{2}(1 - s(t))\Big(n\hat{\mathbb{1}} - \sum_{j=1}^{n} \hat{\sigma}_x^{(j)}\Big) + s(t)\Big(\hat{\mathbb{1}} - |m\rangle\langle m|\Big). \tag{2.16}$$

Roland and Cerf [15] demonstrate that a linear schedule function $s^{(l)}(\tau) = \tau = t/t_f$ does not produce a quantum speed up and it is necessary to use a more efficient non-linear $s(\tau)$, whose rate of change is in proportion to the size of the gap $g(t)$ at that point in the schedule, in order to produce the quadratic speed up of Grover's search algorithm. It remains to specify the function $s(\tau)$ for the optimal performance of this Hamiltonian for searching. In the regime of limited running time, the schedule $s(\tau)$ may be optimized to minimize the error.

A more quantitative statement of the adiabatic theorem [4] [15] proceeds as follows: Consider a time-dependent Hamiltonian of the form in equation (2.16), with initial and final Hamiltonians $\hat{H}_0$, $\hat{H}_p$ respectively, and parametrized by the schedule function $s(\tau)$ that sweeps from $s(0) = 0$ to $s(1) = 1$ over a time t_f, the runtime of the sweep. Denote by $|\varepsilon_j(t)\rangle$ the jth energy eigenstate of the Hamiltonian at time t and its energy by $\varepsilon_j(t)$, where $j = 0, 1$ denotes the ground and first excited states respectively. Provided that $\varepsilon_2(t) > \varepsilon_1(t)$ for $t \in [0, t_f]$ and transitions to

higher energy eigenstates can be ignored, the final state obeys

$$| \langle \varepsilon_0(t_f) | \psi(t_f) \rangle |^2 \geq 1 - \epsilon^2 \tag{2.17}$$

for small parameter $\epsilon \ll 1$, provided that at all times

$$\frac{|\langle \frac{d\hat{H}}{dt} \rangle_{0,1}|}{g^2(t)} \leq \epsilon \ll 1 \tag{2.18}$$

where the matrix element $\langle \frac{d\hat{H}}{dt} \rangle_{0,1}$ is given by

$$\left\langle \frac{d\hat{H}}{dt} \right\rangle_{0,1} = \left\langle \varepsilon_0(t) \middle| \frac{d\hat{H}}{dt} \middle| \varepsilon_1(t) \right\rangle \tag{2.19}$$

and the gap $g(t)$ is given by

$$g(t) = \varepsilon_1(t) - \varepsilon_0(t). \tag{2.20}$$

The equation (2.18) is a condition on the instantaneous rate at which probability amplitude will leave the ground state for the first excited state, assuming the first excited state is not populated. We can therefore describe equation (2.18) as a two-level approximation. In the context of the search algorithms studied here, such an approximation turns out to good for all but the smallest values of n, and becomes more accurate for larger search spaces. However, the adiabatic schedules, $s(\tau)$ derived from equation (2.18) are not always optimal. The optimality is lost where transfer from the ground state directly to a higher excited state dominates over, or is competitive with, transfer to the first excited state, as such transitions are not taken into account in equation (2.18).

2.4 Single avoided crossing model

Morley et al. [22] have shown that a single avoided crossing dominates for large N for both QW and AQC search algorithms on the hypercube. Dominance of a single avoided crossing is the method used to solve analytically for all Hamiltonian-based quantum search algorithms treated to date, including the complete graph [15] and Cartesian lattices (which provide a quantum speed up for $d \geq 4$ dimensions) [20]. It is also the typical behavior for a broad class of random search graphs [23]. Morley et al. [22] introduce a simple, two state, single avoided crossing model for quantum search which proves the quadratic quantum speed up across quantum walk to AQC through hybrid intermediate algorithms.

There are several ways to parametrize a two-state single avoided crossing model. If we designate the marked state to be $|0\rangle$, this will be the end point of the schedule. The initial state needs to be orthogonal to $|0\rangle$, i.e., it has to be $|1\rangle$. These two states are the lowest energy eigenstates of $\frac{1}{2}(\hat{\mathbb{1}} - \hat{\sigma}_z)$ and $\frac{1}{2}(\hat{\mathbb{1}} + \hat{\sigma}_z)$ respectively, where the factor of $\frac{1}{2}$ makes the eigenenergies zero and one in our units. We also need a hopping Hamiltonian term $\hat{\sigma}_x$, to drive transitions between $|1\rangle$ and $|0\rangle$. The relative strength of the hopping Hamiltonian is g_{min}, the minimum gap at the avoided crossing. The single avoided crossing AQC search Hamiltonian is

$$\hat{H}_{AC}(t) = (1 - s(t))\hat{H}_0 + s(t)\hat{H}_p, \tag{2.21}$$

$$\hat{H}_0 = \frac{1}{2}(\hat{\mathbb{1}} + \hat{\sigma}_z) - g_{min}\hat{\sigma}_x, \tag{2.22}$$

$$\hat{H}_p = \frac{1}{2}(\hat{\mathbb{1}} - \hat{\sigma}_z). \tag{2.23}$$

The initial state $|1\rangle$ is only an approximate eigenstate of $\hat{H}_0$, but the approximation improves as g_{min} decreases. Solving the eigensystem for this Hamiltonian

gives

$$g_{AC}(t) = \{[1 - 2s(t)]^2 + 4g_{min}^2[1 - s(t)]^2\}^{\frac{1}{2}} \tag{2.24}$$

for the gap between the two energy levels. The minimum gap occurs for $s(t = \frac{t_f}{2}) = \frac{1}{2}$. Morley et al. [22] then apply the method of [15] to find the optimal schedule s(t) for this system.

$$s(t) \simeq \frac{1}{2}\{1 - g_{min}\cot[g_{min}(2\epsilon t + 1)]\}. \tag{2.25}$$

The runtime t_f is given by

$$\epsilon t_f = \frac{\frac{\pi}{2} - \arctan(g_{min})}{g_{min}}. \tag{2.26}$$

The quantum walk form of the single avoided crossing search Hamiltonian is also simple to analyse. We deduce the optimal value of $\gamma_o = 1$ from the value of $s(t = \frac{t_f}{2}) = \frac{1}{2}$ at the avoided crossing, which gives us

$$\hat{H}_{QWS} = \frac{1}{2}(\hat{\mathbb{1}} - g_{min}\hat{\sigma}_x). \tag{2.27}$$

The $\hat{\sigma}_x$ term causes deterministic transitions between the two states regardless of their energies, at a rate determined by g_{min}. By solving for the dynamics, the time for the input state $|1\rangle$ to evolve to the marked state $|0\rangle$ can be shown to be $t_f = \pi/g_{min}$.

2.5 Open quantum system

Following the work of Albash and Lidar [24] [25] we analyse a quantum system evolving in the presence of a thermal bath that is described in terms of an adiabatic master equation with time-dependent Lindblad operators. Consider a time-dependent system Hamiltonian

$$\hat{H}_S(t)|\varepsilon_a(t)\rangle = \varepsilon_a(t)|\varepsilon_a(t)\rangle, \tag{2.28}$$

where the states $\{\varepsilon_a(t)\rangle\}$ are the instantaneous energy eigenstates and the gap is

$$g_{min} \equiv \min_{a,t}(\varepsilon_a(t) - \varepsilon_0(t)) > 0, \tag{2.29}$$

where $|\varepsilon_0(t)\rangle$ is the instantaneous ground state and $|\varepsilon_a(t)\rangle$ $(a \geq 1)$ are the excited states. The condition $g_{min} > 0$ ensures that only excited states that do not eventually become part of the ground subspace are considered. The generic system-bath Hamiltonian is

$$\hat{H}(t) = \hat{H}_S(t) \otimes \hat{\mathbb{1}}_B + \hat{\mathbb{1}}_S \otimes \hat{H}_B + \hat{H}_I \tag{2.30a}$$

$$\hat{H}_I = g \sum_a \hat{A}_\alpha \otimes \hat{B}_\alpha \tag{2.30b}$$

where $\hat{A}_\alpha$ and $\hat{B}_\alpha$ in the interaction Hamiltonian are, respectively, dimensionless Hermitian system and bath operators and g is the system-bath coupling strength. An adiabatic master equation in Lindblad form for the system's evolution can be derived in the weak coupling limit in the sense of equation (2.33a) below by invoking the standard Born-Markov and rotating wave approximations, along with an adiabatic approximation. Consider the bath correlation functions:

$$\mathcal{B}_{\alpha\beta}(t) \equiv e^{i\hat{H}_B t} B_\alpha e^{-i\hat{H}_B t} \hat{B}_\beta, \tag{2.31}$$

The characteristic decay time τ_B is then defined via

$$|\langle \mathcal{B}_{\alpha\beta}(t)\rangle| \equiv |Tr[\rho_B \mathcal{B}_{\alpha\beta}(t)]| \sim e^{-t/\tau_B} \tag{2.32}$$

where ρ_B is the initial state of the bath. Note that this exponential decay is not guaranteed but simply assumed here in order to extract the timescale τ_B. Now assume:

$$g^2\tau_B \ll g_{min} \qquad \text{(weak coupling)} \tag{2.33a}$$

$$g\tau_B \ll 1 \qquad \text{(Markov approximation)} \tag{2.33b}$$

$$\frac{h}{t_f} \ll \min\{g_{min}^2, \tau_B^{-2}\} \tag{2.33c}$$

where $h \equiv \max_{t\in[0,t_f];a,b} |\langle \varepsilon_a(t)|\partial_t H(t)|\varepsilon_b(t)\rangle|$ estimates the rate of change of the Hamiltonian. Inequality (2.33c) combines the heuristic adiabatic approximation with the condition that the instantaneous energy eigenbasis should be slowly varying on the timescale of the bath. Inequality (2.33c) variant of adiabatic theorm is derived in Section III of [25] and can be compared to equations (2.18) and (2.19). Provided these conditions are satisfied, the quantum adiabatic master equation takes the generic form:

$$\frac{d}{dt}\rho_S(t) = -i[\hat{H}_S(t) + \hat{H}_{LS}(t), \rho(t)] + \mathcal{L}[\rho(t)] \tag{2.34a}$$

$$\mathcal{L}[\rho(t)] \equiv \sum_{\omega} \gamma_{\alpha\beta}(\omega)\Big(\hat{L}_{\beta,\omega}(t)\rho(t)\hat{L}^\dagger_{\alpha,\omega} - \frac{1}{2}\{\hat{L}^\dagger_{\alpha,\omega}(t)\hat{L}_{\beta,\omega}(t), \rho(t)\}\Big), \tag{2.34b}$$

where the sum over ω is over the Bohr frequencies of H_S, and where the time-dependent Lindblad operators are

$$\hat{L}_{\alpha,\omega}(t) = \sum_{\omega=\varepsilon_b(t)-\varepsilon_a(t)} \langle \varepsilon_a(t)|\hat{A}_\alpha|\varepsilon_b(t)\rangle |\varepsilon_a(t)\rangle\langle\varepsilon_b(t)|. \tag{2.35}$$

The derivation of these master equations is provided in Section IV(C) and Appendix G of [25]. The decay rates

$$\gamma_{\alpha\beta}(\omega) = g^2 \int_{\infty}^{-\infty} dt\, e^{i\omega t} \langle \mathcal{B}_{\alpha\beta}(t) \rangle \tag{2.36}$$

are Fourier transforms of the bath correlation function forming a positive matrix $\gamma(\omega)$ whose elements satisfy the KMS condition

$$\gamma_{\alpha\beta}(-\omega) = e^{-\beta\omega} \gamma_{\beta\alpha}(\omega) \tag{2.37}$$

where β is the inverse temperature, and

$$\hat{H}_{LS} = \sum_{\alpha\beta} \sum_{\omega} S_{\alpha\beta}(\omega) \hat{L}^{\dagger}_{\alpha,\omega}(t) \hat{L}_{\beta,\omega}(t), \tag{2.38}$$

is a Lamb shift term, where

$$S_{\alpha\beta}(\omega) = \int_{\infty}^{-\infty} d\omega'\, \gamma_{\alpha\beta}(\omega')\, \mathcal{P}\Big(\frac{1}{\omega - \omega'}\Big) \tag{2.39}$$

with $\mathcal{P}$ denoting the Cauchy principal value.

Chapter 3

Open quantum system for quantum walk search

3.1 Analytics

We consider the weak coupling limit as follows from equation (2.33a) and the quasi-intermediate coupling regime where g is comparable to g_{min}. This approach works under the approximation that the characteristic bath decay time τ_B is very small and hence satisfies the equation (2.33b) and thus equation (2.33a). Using the master equation formalism, we have traced out the bath and only consider the system dynamics. Specifically consider

$$\hat{H}_S = \frac{1}{2}(\hat{\mathbb{1}} - \omega_x \hat{\sigma}^x),\ \hat{H}_I = g\hat{\sigma}^z \otimes \hat{B},\ \omega_x = g_{min}, \tag{3.1}$$

where g is the coupling strength between the system and the bath. The interaction Hamiltonian, $\hat{H}_I$ is so chosen for three basic reasons, (i) $[\hat{H}_S, \hat{H}_I] \neq 0$ has to be followed to observe decoherence effects; (ii) the eigenvectors of $\hat{\sigma}^z$ form the computational basis and hence provides mathematical convenience; (iii) collective dephasing

is experimentally achievable. We change the minimum energy gap, g_{min} to ω_x for convenience in analytical calculations.

The energy eigenstates of $\hat{H}_S$ are $|\varepsilon_0\rangle = |+\rangle$ and $|\varepsilon_1\rangle = |-\rangle$ with respective eigenvalues $-\frac{1}{2}\omega_x$ and $\frac{1}{2}\omega_x$, where $|\pm\rangle = \frac{1}{\sqrt{2}}(|0\rangle \pm |1\rangle)$. Since $\hat{\sigma}_z|\pm\rangle = |\mp\rangle$,using equation (2.35) the non-zero Lindblad operators are:

$$\hat{L}_{z,\omega_x} = |+\rangle\langle -|,\ \hat{L}_{z,-\omega_x} = |-\rangle\langle +|. \tag{3.2}$$

Note that now we have a non-trivial Lamb shift term:

$$\hat{H}_{LS} = S(\omega_x)|-\rangle\langle -| + S(-\omega_x)|+\rangle\langle +|. \tag{3.3}$$

We consider the decay rates :

$$\gamma(\omega) = \frac{g^2\omega}{\omega^2 + 1}. \tag{3.4}$$

The decay rates chosen are the ohmic bath spectral density using the Druid-Lorentz cutoff to avoid divergent integrals for the Lamb shift term. The simplicity of the decay rates is to ensure mathematical convenience for analytical and numerical calculations. Using equations (3.4),(2.37) and (2.39), we can get all the corresponding needed values for decay rates and Lamb shift terms. For solving this in the energy eigenbasis, the matrix form of Lamb shift term, Lindblad operators and system Hamiltonian is:

$$\hat{H}_{LS} = \begin{pmatrix} S(-\omega_x) & 0 \\ 0 & S(\omega_x) \end{pmatrix}, \tag{3.5}$$

$$\hat{L}_{z,\omega_x} = \begin{pmatrix} 0 & 1 \\ 0 & 0 \end{pmatrix}, \tag{3.6}$$

$$\hat{L}_{z,-\omega_x} = \begin{pmatrix} 0 & 0 \\ 1 & 0 \end{pmatrix}, \tag{3.7}$$

$$\hat{H}_S = \begin{pmatrix} \frac{-\omega_x}{2} & 0 \\ 0 & \frac{\omega_x}{2} \end{pmatrix}, \tag{3.8}$$

Substituting equations (3.1)-(3.4) in equation (2.34), we get

$$[\hat{H}_S(t) + \hat{H}_{LS}, \rho(t)] \equiv \begin{pmatrix} 0 & \rho_{+-}(S(-\omega_x) - S(\omega_x) - \omega_x) \\ \rho_{-+}(S(\omega_x) - S(-\omega_x) + \omega_x) & 0 \end{pmatrix} \tag{3.9}$$

$$\mathcal{L}[\rho(t)] \equiv \gamma(\omega_x) \begin{pmatrix} \rho_{--} & -\rho_{+-}/2 \\ -\rho_{-+}/2 & -\rho_{--} \end{pmatrix} + \gamma(-\omega_x) \begin{pmatrix} -\rho_{++} & -\rho_{+-}/2 \\ -\rho_{-+}/2 & \rho_{++} \end{pmatrix} \tag{3.10}$$

We find that the master equations for the density matrix components are:

$$\frac{d}{dt}\rho_{--}(t) = -\gamma(\omega_x)\rho_{--}(t) + \gamma(-\omega_x)\rho_{++}(t), \tag{3.11a}$$

$$\frac{d}{dt}\rho_{++}(t) = \gamma(\omega_x)\rho_{--}(t) - \gamma(-\omega_x)\rho_{++}(t), \tag{3.11b}$$

$$\frac{d}{dt}\rho_{-+}(t) = \frac{d}{dt}\rho^*_{+-}(t) = \Big[-i(S(\omega_x) - S(-\omega_x) + \omega_x) - \frac{1}{2}\gamma(\omega_x)(1 + e^{-\beta\omega_x}) \Big] \rho_{-+}(t), \tag{3.11c}$$

where we have used the KMS condition to simplify the expressions. These equations can be solved analytically to give:

$$\rho_{-+}(t) = \rho_{-+}(0) e^{-i(S(\omega_x) - S(-\omega_x) + \omega_x)t} e^{-t/T_2^{(e)}} \tag{3.12a}$$

$$\rho_{--}(t) = p_{Gibbs}(-) + [\rho_{--}(0) - p_{Gibbs}(-)] e^{-t/T_1^{(e)}} \tag{3.12b}$$

$$\rho_{++}(t) = 1 - \rho_{--}(t), \qquad \rho_{+-}(t) = \rho^*_{-+}(t), \tag{3.12c}$$

where

$$p_{Gibbs}(\pm) = \frac{e^{\pm\beta\omega_x/2}}{Z}, Z = e^{\beta\omega_x/2} + e^{-\beta\omega_x/2}, \tag{3.13}$$

and

$$T_1^{(e)} = \frac{1}{\gamma(\omega_x)(1+e^{-\beta\omega_x})}, \;\; T_2^{(e)} = 2T_1^{(e)}. \tag{3.14}$$

We observe three important facts about the result in equation (3.12). First, the decoherence occurs in the energy eigenbasis, i.e., the off-diagonal components *in the energy eigenbasis* (hence the 'e' superscripts on $T1$ and $T2$) decay exponentially to zero with a timescale determined by $T_2^{(e)}$, and this includes the entire contribution of the Lamb shift. Second, the populations $(\rho_{++}; \rho_{--})$ approach the Gibbs state associated with the Hamiltonian H_S within a timescale determined by $T_1^{(e)}$. Third, the two timescales $(T_1^{(e)}; T_2^{(e)})$ have a non-trivial dependence on the energy gap ω_x, coupling strength, g and the inverse temperature, β.

Using equation (3.12), in the computational basis, we get the probability to be in the ground state of the system to be

$$\rho_{00}(t) = P(t) = \frac{1}{2}(1 - e^{\frac{-t}{T_2}} \cos(St)) \tag{3.15}$$

where,

$$S = S(\omega_x) - S(-\omega_x) + \omega_x \tag{3.16}$$

Now for,

$$\frac{d\rho_{00}}{dt} = 0 \tag{3.17}$$

gives us the maximas and minimas of the equation, and,

$$\frac{d^2\rho_{00}}{dt^2} < 0 \tag{3.18}$$

makes sure that the value found is the maxima. Solving the above equations, we

get the time to reach the peak probability for the first time, t_{p1},

$$t_{p1} = \frac{1}{S}\left[k\pi - \arctan\left[\frac{-1}{T_2 S}\right]\right] \tag{3.19}$$

$$t_{p1} > \frac{1}{S}\arctan\left[\frac{1}{2}\left[T_2 S - \frac{1}{T_2 S}\right]\right] \tag{3.20}$$

where, $S = S(\omega_x) - S(-\omega_x) + \omega_x$ and k is the smallest whole number for which equation (3.19) and (3.20) hold true.

Please check Appendix A for the full expansion of $S(\omega_x)$ and $S(-\omega_x)$.

3.2 Numerical Analysis

Following the analytical calculations, we want to observe numerically, the dynamics of a quantum walk search algorithm for a two level system in a thermal bath. We use *Python*3 to perform the calculations and the numerical integration for the Lamb shift terms provided in Appendix A to get the results and generate the plots. Built-in functions from the *Numpy* and *Scipy* libraries are used and the accuracy of the results depend on the accuracy of the integral functions. We see in equation (3.15) that the probability to reach the ground state of the system depends upon the runtime, the coupling strength, the temperature and the minimum energy gap. According to equations (3.19) and (3.20), the time needed to reach the peak of the probability function for the first time, depends on the coupling strength, the temperature and the minimum energy gap. Next, we vary these three parameters along with appropriate runtime to observe the dynamics of the system under different operating conditions.

Firstly, we want to know in what range of coupling strengths is our model going to be valid. This valid range of coupling strength is dependent on the temperature

and the value of g_{min}. We fix the inverse temperature, β and g_{min} in different regimes and observe. In figure 3.1(a), at very low temperatures and relatively higher g_{min}

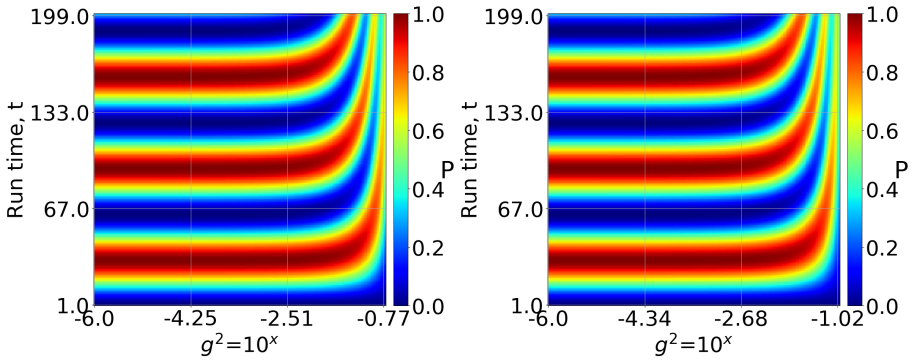

(a) $\beta = 10000, g_{min} = 0.1$

(b) $\beta = 0.0001, g_{min} = 0.1$

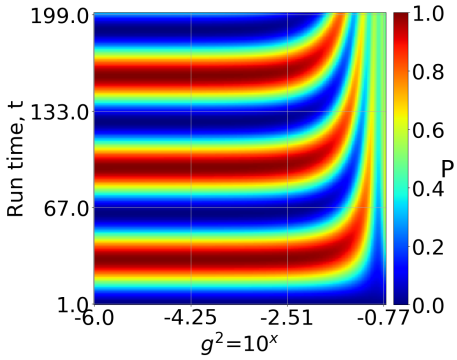

(c) $\beta = 1, g_{min} = 0.1$

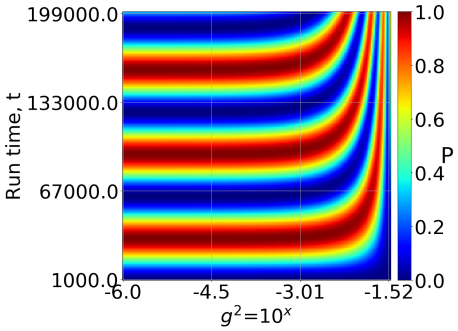

(d) $\beta = 1, g_{min} = 0.0001$

Figure 3.1: Plotting probability, P of being in ground state of quantum walk search Hamiltonian in computational basis in an ohmic bath while varying coupling strength, g^2 vs runtime, t for specified values of inverse temperature, β and minimum energy gap, g_{min}. The single avoided crossing model describing a two-level approximation of multi-qubit quantum walk search in presence of an ohmic bath is being analysed. The plots provide an outlook on the valid ranges of coupling strength under different values of the parameters.

we can observe that the weak coupling approximation for the model starts breaking down close to $g^2 = 10^{-0.75}$. For high temperature and similar g_{min}, in figure 3.1(b), we observe the validity regime of coupling strength shifts to lower values as the decoherence due to temperature effects takes effect. In figure 3.1(c) and 3.1(d), we are at intermediate temperature and we observe that for smaller energy gap (larger number of qubits) the validity regime of coupling strength shifts to lower values, this follows according to the weak coupling and the Markov approximation of the open quantum systems, equations (2.33a) and (2.33b). For the following plots, we aim

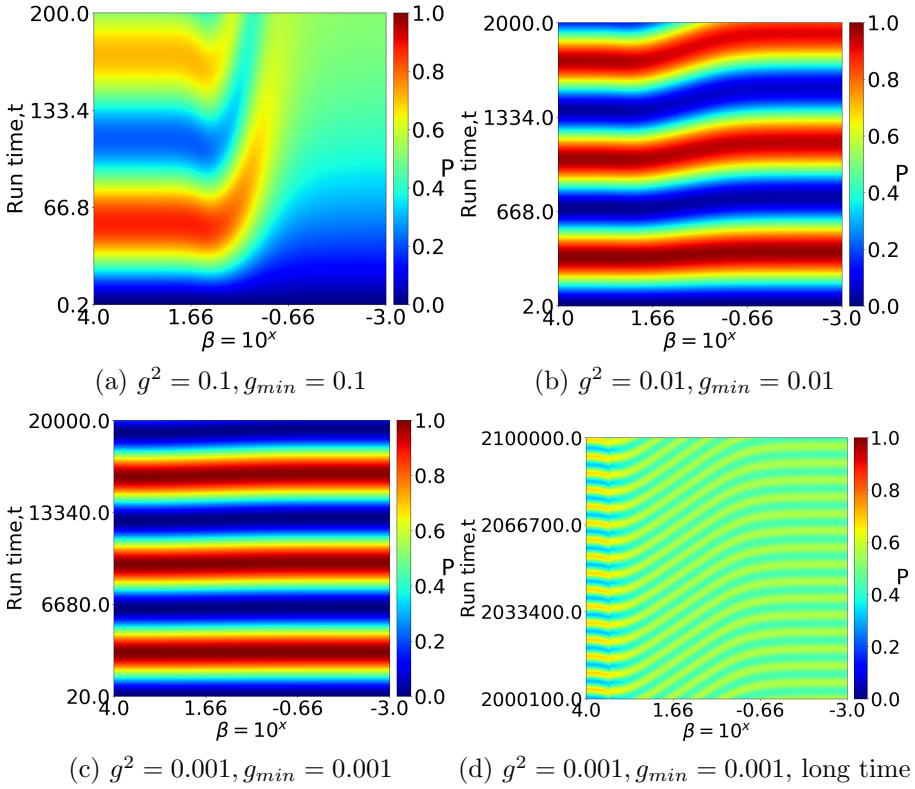

(a) $g^2 = 0.1, g_{min} = 0.1$ (b) $g^2 = 0.01, g_{min} = 0.01$

(c) $g^2 = 0.001, g_{min} = 0.001$ (d) $g^2 = 0.001, g_{min} = 0.001$, long time

Figure 3.2: Plotting probability, P of being in ground state of quantum walk search Hamiltonian in computational basis in an ohmic bath while varying inverse temperature, β vs runtime, t for specified values of coupling strength, g^2 and minimum energy gap, g_{min}. The single avoided crossing model describing a two-level approximation of multi-qubit quantum walk search in presence of an ohmic bath is being analysed. The plots provide an outlook on the performance of search algorithm at different temperatures for specified values of other parameters.

to stay in the validity regime to observe proper dynamics according to our single avoided crossing model. In figure 3.2, we aim to observe dynamics of the probability of the ground state, $P(t)$, for fixed values of g_{min} and coupling strength within the range of validity, while varying the inverse temperature and runtime. We observe in figure 3.2(a), at high coupling strength and relatively high g_{min}, the decoherence has a large impact at higher temperatures and the search does no better than guessing ($P = 0.5$), while at lower temperatures, even at such high coupling with the bath, we can gain solution for the search problem with moderately good probability for the first few peaks. For the search problem, we normally aim to get our solution on the first peak.

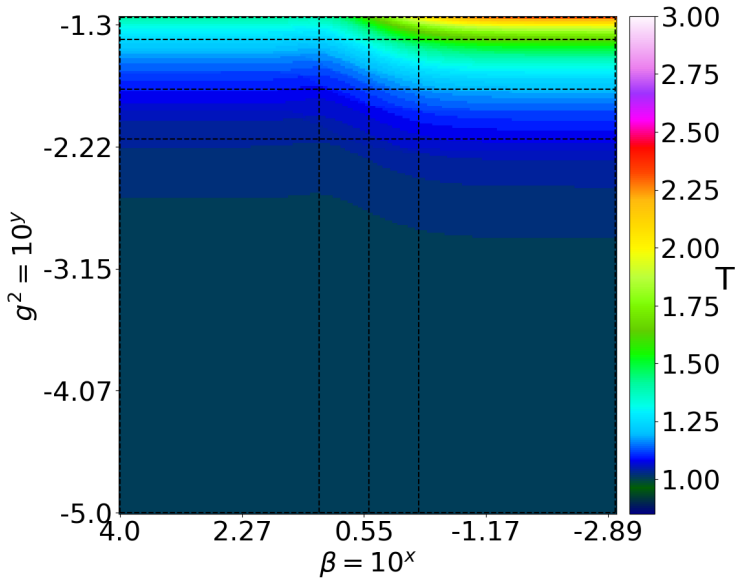

(a) $g_{min} = 0.1, g^2\, vs\, \beta$

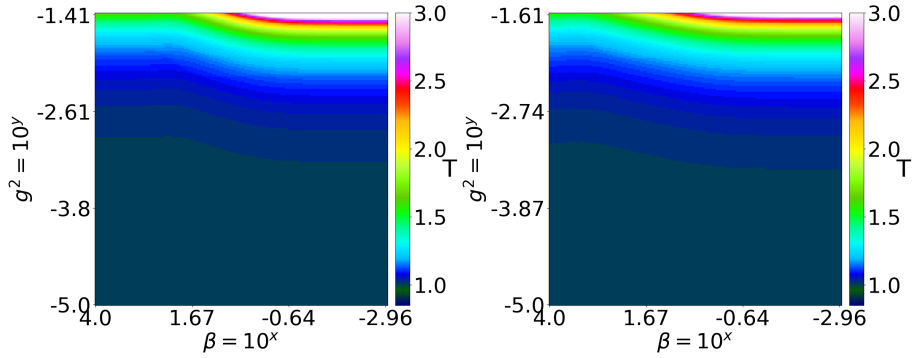

(b) $g_{min} = 0.01, g^2\, vs\, \beta$

(c) $g_{min} = 0.001, g^2\, vs\, \beta$

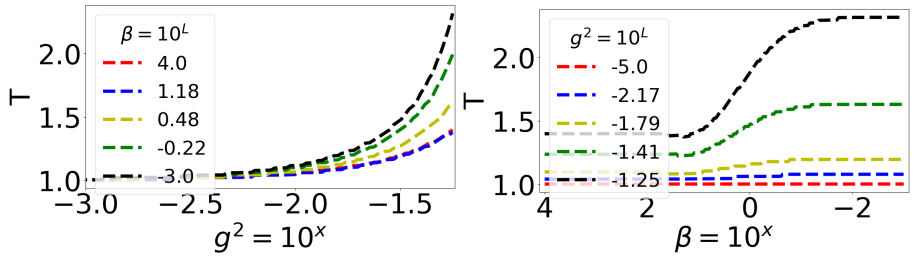

(d) $g_{min} = 0.1, T\, vs\, g^2$

(e) $g_{min} = 0.1, T\, vs\, \beta$

Figure 3.3: Plotting cost factor, T while varying coupling strength, g^2 vs inverse temperature, β for the first peak of probability, P of being in ground state of quantum search Hamiltonian in computational basis and specified minimum energy gap, g_{min} to describe how worse off the search algorithm is performing in the presence of an ohmic bath, compared to the best theoretical time to get the solution predicted by the two-level approximation in absence of the bath. The 2-d slice plots (d) and (e) provide a clearer picture of the cost factor variation at different values of the parameters. The single avoided crossing model describing a two-level approximation of multi-qubit quantum walk search in presence of an ohmic bath is being analysed.

For the following plots, we aim to stay in the validity regime to observe proper dynamics according to our single avoided crossing model. In figure 3.2, we aim to observe dynamics of the probability of the ground state, $P(t)$, for fixed values of g_{min} and coupling strength within the range of validity, while varying the inverse temperature and runtime. We observe in figure 3.2(a), at high coupling strength and relatively high g_{min}, the decoherence has a large impact at higher temperatures and the search does no better than guessing ($P = 0.5$), while at lower temperatures, even at such high coupling with the bath, we can gain solution for the search problem with moderately good probability for the first few peaks. For the search problem, we normally aim to get our solution on the first peak. In figure 3.2(b) and 3.2(c), while the temperature effects are there, they become less prevalent on short time scales at increasingly lower coupling strengths. While on long time scales, as in figure 3.2(d), we can see the temperature effects are strongly present, where at lower temperature, the algorithm can still provide solution with moderately good probability.

An important factor we consider while examining the performance of an algorithm is the cost factor. The cost factor is used to describe how worse off are we performing from the best theoretical predicted time to get the solution. Here, we define the cost factor, T as

$$T = \frac{t_m g_{min}}{\pi P_m} \tag{3.21}$$

where, t_m refers to the runtime taken to reach the first peak of the quantum walk and P_m refers to the maximum probability at that peak. We scale this with $\frac{g_{min}}{\pi}$, inverse of the best theoretical predicted time for the walk.

In figure 3.3, we color plot the cost factor, T for coupling strength, g^2 vs inverse temperature, β for fixed values of minimum energy gap g_{min}. Recalling equation (2.15), the minimum energy gap g_{min} is inversely proportional to square root of the number of basis states which depend upon the number of qubits. We observe the worsening of the performance of with increasing coupling strength with the bath and increasing temperature.

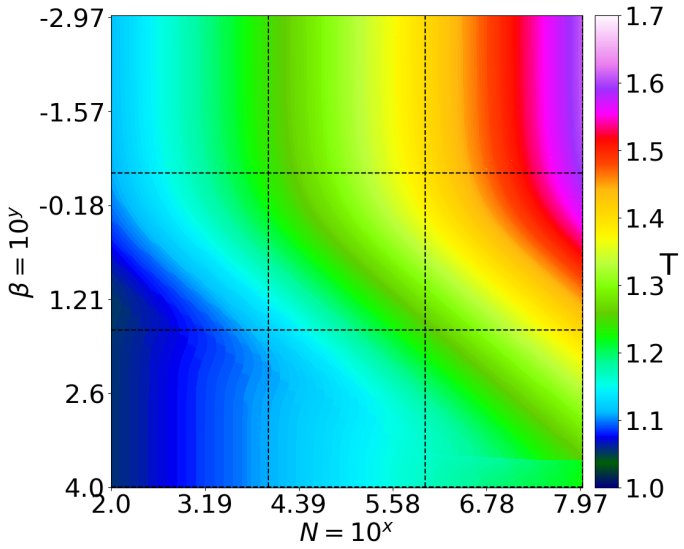

(a) $g^2 = 0.01, g_{min}\, vs\, \beta$

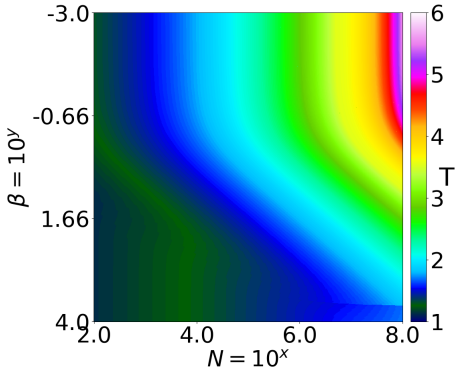

(b) $g^2 = 0.0225, g_{min}\, vs\, \beta$

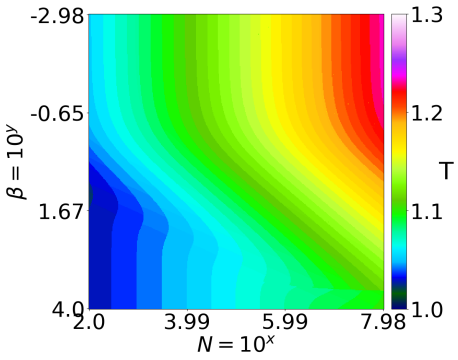

(c) $g^2 = 0.005, g_{min}\, vs\, \beta$

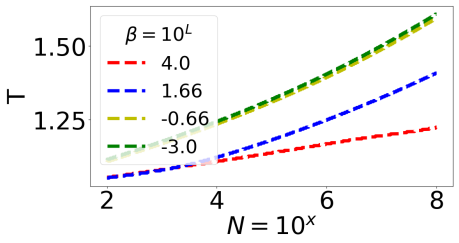

(d) $g^2 = 0.01, T\, vs\, N$

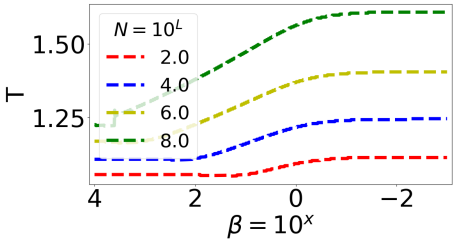

(e) $g^2 = 0.01, T\, vs\, \beta$

Figure 3.4: Plotting cost factor, T while varying inverse temperature, β vs number of basis states, N for the first peak of probability, P of being in ground state of quantum search Hamiltonian in computational basis for specified values of coupling strength, g^2 to describe how worse off the search algorithm is performing in the presence of an ohmic bath, compared to the best theoretical time to get the solution predicted by the two-level approximation in absence of the bath. Note the colour scales for T are different in each sub-figure. The 2-d slice plots (d) and (e) provide a clearer picture of the cost factor variation at different values of the parameters. The single avoided crossing model describing a two-level approximation of multi-qubit quantum walk search in presence of an ohmic bath is being analysed.

We also see that for similar coupling strength and temperature, the performance seems to be worse with increasing qubits. This fact will be demonstrated better in the next figure. We plot vertical and horizontal slices from figure 3.3(a) as figure 3.3(d) and 3.3(e). They emphasise our analysis much better. This follows directly from equation (3.19) and (3.20), with lower coupling strength, the Lamb shift becomes more trivial and the $T_2^{(e)}$ time scale becomes increasingly larger, with the term $T_2 S$ becoming larger. Thus the cost factor becomes smaller and very close to 1.

In figure 3.4, we address the final point of our problem, how does cost factor vary due to the changes in temperature and the number of qubits. As in figure 3.4(b), we observe that at relatively higher coupling strengths, the model easily starts breaking down with increasing number of qubits and the cost factor being high. This is due to the Lamb shift Hamiltonian starting to compete and even dominating over the system Hamiltonian where the model breaks down. We can observe that, at the same temperature, with increasing number of qubits, the performance of the system worsens, and the system is affected by the environment much more easily. And as we observed earlier, for a particular size of the system, with increase in temperature, the performance worsens.

There is a particular feature we have observed in our plots which can be issue for further research. There is a peaking behaviour of the cost factor, where we observe that its not the case, lower the temperature, the better the performance. The performance seems to be optimal at a particular optimal temperature for a given system size and coupling strength, higher or lower temperature gives worse results. Figure 3.4(c) shows this especially clearly, with the optimal temperature decreasing for increasing system size (lower g_{min}). We are not sure whether this is a nuance of the numerics of this particular model, or a general feature in performance of this class of algorithms.

Chapter 4

Open quantum system for adiabatic quantum computation

4.1 Analytics

We consider the weak coupling limit as follows from equation (2.33a) and the quasi-intermediate coupling regime where g is comparable to g_{min}. This approach works under the approximation that the characteristic bath decay time τ_B is very small and hence satisfies the equation (2.33b) and thus equation (2.33a). Using the master equation formalism, we have traced out the bath and only consider the system dynamics. Specifically consider

$$\hat{H}_S(t) = (1 - s(t))\hat{H}_0 + s(t)\hat{H}_p, \tag{4.1}$$

$$\hat{H}_0 = \frac{1}{2}(\hat{\mathbb{1}} + \hat{\sigma}_z) - g_{min}\hat{\sigma}_x, \tag{4.2}$$

$$\hat{H}_p = \frac{1}{2}(\hat{\mathbb{1}} - \hat{\sigma}_z), \tag{4.3}$$

where $\hat{H}_0$ is the driver Hamiltonian and $\hat{H}_p$ is the problem Hamiltonian, non-linear $s(t)$ for optimal performance is

$$s(t) \simeq \frac{1}{2}\{1 - g_{min}\cot[g_{min}(2\epsilon t + 1)]\}. \tag{4.4}$$

The runtime t_f is given by

$$\epsilon t_f = \frac{\frac{\pi}{2} - \arctan(g_{min})}{g_{min}}. \tag{4.5}$$

The system-bath interaction Hamiltonian is defined as

$$\hat{H}_I = g\hat{\sigma}^z \otimes \hat{B}, \tag{4.6}$$

where g is the coupling strength between the system and the bath. The interaction Hamiltonian, $\hat{H}_I$ is so chosen for three basic reasons, (i) $[\hat{H}_S, \hat{H}_I] \neq 0$ has to be followed to observe decoherence effects; (ii) the eigenvectors of $\hat{\sigma}^z$ form the computational basis and hence provides mathematical convenience; (iii) collective dephasing is experimentally achievable.

Let's redefine the time dependent energy gap, equation (2.24), as

$$\Delta(t) = \{(1 - 2s(t))^2 + 4g_{min}^2(1 - s(t))^2\}^{\frac{1}{2}}. \tag{4.7}$$

This redefinition is done to avoid confusion with coupling strength, g by having an energy gap of form $g(t)$ as in equation (2.24). The energy eigenstates of H_S are

$$|\varepsilon_0(t)\rangle = \frac{1}{\sqrt{2}}\left[\frac{\frac{1}{2} - s(t) - \frac{\Delta(t)}{2}}{g_{min}(-1 + s(t))}|0\rangle + |1\rangle\right] \tag{4.8}$$

and

$$|\varepsilon_1(t)\rangle = \frac{1}{\sqrt{2}}\left[\frac{\frac{1}{2} - s(t) + \frac{\Delta(t)}{2}}{g_{min}(-1+s(t))}|0\rangle + |1\rangle\right] \tag{4.9}$$

with respective eigenvalues $\frac{1}{2}[1-\Delta(t)]$ and $\frac{1}{2}[1+\Delta(t)]$. Using equation (2.35), the non-zero Lindblad operators are

$$\hat{L}_{z,\Delta(t)} = |\varepsilon_0(t)\rangle\langle\varepsilon_1(t)|\,,\ \hat{L}_{z,-\Delta(t)} = |\varepsilon_1(t)\rangle\langle\varepsilon_0(t)|\,. \tag{4.10}$$

We have a non-trivial Lamb shift term:

$$\hat{H}_{LS} = S(\Delta(t))\,|\varepsilon_1(t)\rangle\langle\varepsilon_1(t)| + S(-\Delta(t))\,|\varepsilon_0(t)\rangle\langle\varepsilon_0(t)|\,. \tag{4.11}$$

We consider the decay rates :

$$\gamma(\omega) = \frac{g^2\omega}{\omega^2+1}. \tag{4.12}$$

The decay rates chosen are the ohmic bath spectral density using the Druid-Lorentz cutoff to avoid divergent integrals for the Lamb shift term. The simplicity of the decay rates is to ensure mathematical convenience for analytical and numerical calculations. Let's define,

$$\lambda_\pm = \frac{\pm(1-2s(t)) + \Delta(t)}{g_{min}(-1+s(t))}. \tag{4.13}$$

Using equations (4.12),(2.37) and (2.39), we can get all the corresponding needed values for decay rates and Lamb shift terms. For solving this in the energy or computational eigenbasis, the matrix form of Lamb shift term, Lindblad

operators and system Hamiltonian is:

$$\hat{H}_{LS}^{(e)} = \begin{pmatrix} S(-\Delta(t)) & 0 \\ 0 & S(\Delta(t)) \end{pmatrix}, \tag{4.14}$$

$$\hat{H}_{LS}^{(c)} = \begin{pmatrix} [1+\frac{\lambda_+^2}{4}]S(\Delta(t)) + [1+\frac{\lambda_-^2}{4}]S(-\Delta(t)) & \frac{\lambda_+ + \lambda_-}{2}(S(\Delta(t)) - S(-\Delta(t))) \\ \frac{\lambda_+ + \lambda_-}{2}(S(\Delta(t)) - S(-\Delta(t))) & [1+\frac{\lambda_-^2}{4}]S(\Delta(t)) + [1+\frac{\lambda_+^2}{4}]S(-\Delta(t)) \end{pmatrix} \tag{4.15}$$

$$\hat{L}_{z,\Delta(t)}^{(e)} = \begin{pmatrix} 0 & 1 \\ 0 & 0 \end{pmatrix}, \quad \hat{L}_{z,\Delta(t)}^{(c)} = \frac{1}{2}\begin{pmatrix} 2 & \frac{-1+2s(t)+\Delta(t)}{g_{min}(-1+s(t))} \\ \frac{1-2s(t)+\Delta(t)}{g_{min}(-1+s(t))} & -2 \end{pmatrix} \tag{4.16}$$

$$\hat{L}_{z,-\Delta(t)}^{(e)} = \begin{pmatrix} 0 & 0 \\ 1 & 0 \end{pmatrix}, \quad \hat{L}_{z,-\Delta(t)}^{(c)} = \frac{1}{2}\begin{pmatrix} 2 & \frac{1-2s(t)+\Delta(t)}{g_{min}(-1+s(t))} \\ \frac{-1+2s(t)+\Delta(t)}{g_{min}(-1+s(t))} & -2 \end{pmatrix} \tag{4.17}$$

$$\hat{H}_S^{(e)} = \begin{pmatrix} \frac{1}{2} + g_{min}(-1+s(t)) & \frac{1}{2} - s(t) \\ \frac{1}{2} - s(t) & \frac{1}{2} - g_{min}(-1+s(t)) \end{pmatrix}, \tag{4.18}$$

$$\hat{H}_S^{(c)} = \begin{pmatrix} 1 - s(t) & -g_{min}(1-s(t)) \\ -g_{min}(1-s(t)) & s(t) \end{pmatrix}. \tag{4.19}$$

In equations (4.14)-(4.19), the superscript (e) denotes representation in energy eigenbasis and the superscript (c) denotes the computational basis. Solving in the energy eigenbasis, we find that the master equations for the density matrix compo-

nents are:

$$\frac{d}{dt}\rho_{00}^{(e)}(t) = \gamma(\Delta(t))\rho_{11}^{(e)}(t) - \gamma(-\Delta(t))\rho_{00}^{(e)}(t) + i[\rho_{01}^{(e)}(t) - \rho_{10}^{(e)}(t)](-\frac{1}{2} + s(t)), \tag{4.20}$$

$$\frac{d}{dt}\rho_{11}^{(e)}(t) = -\gamma(\Delta(t))\rho_{11}^{(e)}(t) + \gamma(-\Delta(t))\rho_{00}^{(e)}(t) + i[\rho_{10}^{(e)}(t) - \rho_{01}^{(e)}(t)](-\frac{1}{2} + s(t)), \tag{4.21}$$

$$\begin{aligned}\frac{d}{dt}\rho_{10}^{(e)}(t) = \frac{d}{dt}\rho_{01}^{(e)*}(t) = \Big[- i(S(\Delta(t)) - S(-\Delta(t)) + 2g_{min}) - \frac{1}{2}(\gamma(\Delta(t)) + \gamma(-\Delta(t)))\Big]\rho_{10}^{(e)}(t) \\ +i(-\frac{1}{2} + s(t))[\rho_{11}^{(e)}(t) - \rho_{00}^{(e)}(t)].\end{aligned} \tag{4.22}$$

Equations (4.20)-(4.22) at $s(t) = \frac{1}{2}$ are equivalent to equation (3.11) describing the quantum walk in energy eigenbasis. Transforming equations (4.20)-(4.22) to the computational basis, the master equation describing the ground state $|0\rangle$ is

$$\begin{aligned}\frac{d}{dt}\rho_{00}^{(c)}(t) = i[\rho_{01}^{(c)}(t) - \rho_{10}^{(c)}(t)][\frac{1}{2}[\lambda_+ + \lambda_-][S(-\Delta(t)) - S(\Delta(t))] + g_{min}[1 - s(t)]] \\ +\frac{1}{4}\gamma(\Delta(t))[-\lambda_+^2\rho_{00}^{(c)}(t) + (\lambda_+ + \lambda_-)[\rho_{01}^{(c)}(t) + \rho_{10}^{(c)}(t)] + \lambda_-^2\rho_{11}^{(c)}(t)] \\ +\frac{1}{4}\gamma(-\Delta(t))[-\lambda_-^2\rho_{00}^{(c)}(t) + (\lambda_+ + \lambda_-)[\rho_{01}^{(c)}(t) + \rho_{10}^{(c)}(t)] + \lambda_+^2\rho_{11}^{(c)}(t)]\end{aligned} \tag{4.23}$$

The master equations for other terms in computational basis are provided in Appendix B.

4.2 Simulations

Following the analytical calculations, we want to observe numerically, the dynamics of an adiabatic quantum computation search algorithm for a two level system in a thermal bath. We solve equation (4.23) and the density matrix components in Appendix B describing the quantum state using the superoperator approach and

solving individual terms using numerical integration. We write the code for this in *Python*3 using built-in functions provided in the *Numpy* and the *Scipy* libraries for performing matrix calculations and numerical integration. The accuracy is limited by the performance of the *Numpy* and *Scipy* libraries with integrals diverging easily for large or really small values of the parameters. Using more robust calculation methods to increase the range of study is in plan for the future work. The plots were generated using the available results in *Python*3.

The equation (4.23) describes the instantaneous probability, $P(t)$ of the ground state $|0\rangle$. The probability to reach the instantaneous ground state of the system depends upon the final runtime, the coupling strength, the temperature and the minimum energy gap. For the all our simulations, we plot for $P(t_f)$, the probability of the ground state $|0\rangle$ at the end of designated AQC scheduled runtime, t_f. Next, we vary these four parameters to observe the dynamics of the system under different operating conditions. Unlike the quantum walk case, the choice of length of final runtime affects the dynamics of AQC significantly.

Firstly, we want to know in which coupling regime our model is going to be valid. The valid range of coupling strength is dependent on the choice of final runtime, the temperature and the g_{min}. We fix the inverse temperature, β and the minimum energy gap, g_{min} and vary the final runtime in different regimes and observe.

In figure 4.1(c), we can observe that, at really low temperatures while the system remains largely unaffected even at relatively stronger coupling strengths, with decrease in g_{min} or conversely increase in the number of qubits, the weak coupling approximation for the system starts breaking down at stronger coupling strengths for shorter runtimes and for larger system size, even at longer runtimes.
In figure 4.1(a) and 4.1(b), we can observe the breakdown of the weak coupling approximation for the system at relatively stronger coupling strength for intermediate temperatures.

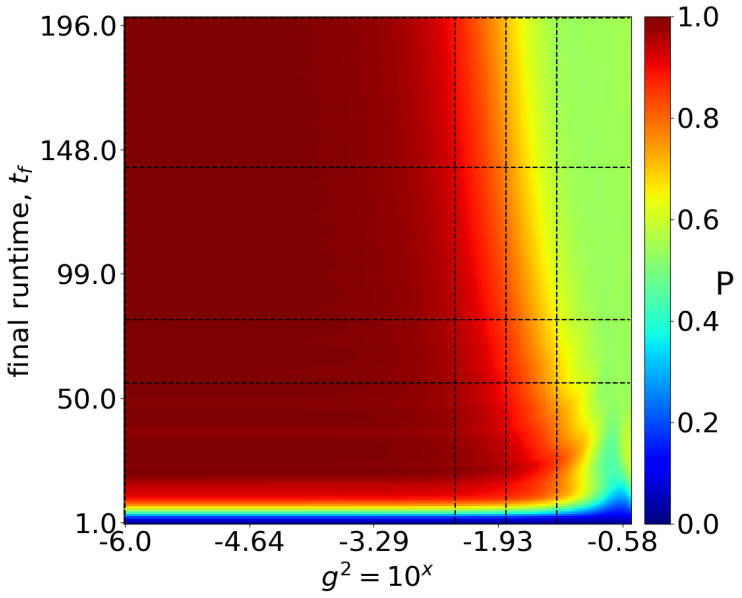

(a) $\beta = 1, g_{min} = 0.1, g^2\ vs\ t_f$

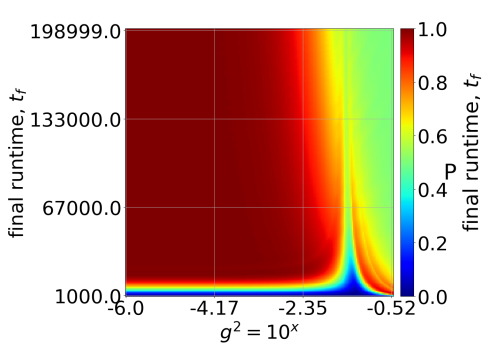

(b) $\beta = 1, g_{min} = 0.0001, g^2\ vs\ t_f$

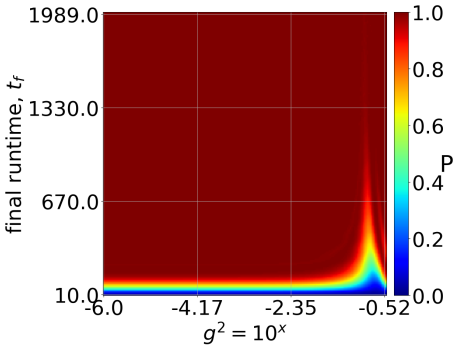

(c) $\beta = 10000, g_{min} = 0.01, g^2\ vs\ t_f$

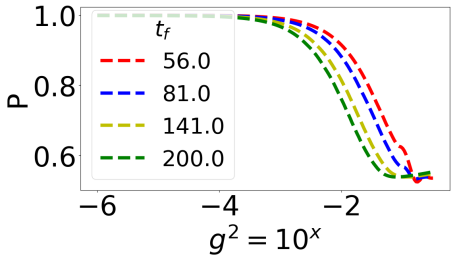

(d) $\beta = 1, g_{min} = 0.1, g^2\ vs\ P$

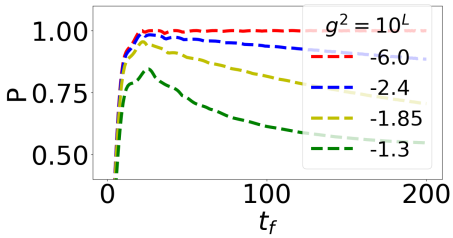

(e) $\beta = 1, g_{min} = 0.1, t_f\ vs\ P$

Figure 4.1: Plotting probability, $P(t_f)$ of being in instantaneous ground state of the AQC search Hamiltonian in computational basis while varying coupling strength, g^2 vs final runtime, t_f for specified values of inverse temperature, β and minimum energy gap, g_{min}. The 2-d slice plots (d) and (e) provide a clearer picture of the variation of $P(t_f)$ at different values of the parameters. The single avoided crossing model describing a two-level approximation of multi-qubit AQC search in presence of an ohmic bath is being analysed. The plots provide an outlook on the valid ranges of coupling strength under different values of other parameters and show that having longer runtimes to achieve higher success probability may not be suitable in the presence of an ohmic bath.

At this point two factors come into work, the decoherence of the system becomes strong enough to overwhelm the coherent AQC dynamics leading to the system getting thermalized and the Lamb shift Hamiltonian term starts to compete and even overwhelm the system Hamiltonian. Thus, the valid range of the system reduces to lower coupling strengths, with increase in the temperature and the system size. We also observe that for certain range of coupling strengths for a specified temperature and system size, the probability of being in the ground state after the schedule runtime is higher at shorter runtimes, unlike the advocated longer runtimes are better in AQC. The figures 4.1(d) and 4.1(e) are horizontal and vertical slices at specified values of final runtime, t_f and coupling strength, g^2 in figure 4.1(a). They aim to better exhibit the discussed observations.

For the following plots, we aim to stay in the validity regime to observe proper dynamics according to our single avoided crossing model. In figure 4.2, we aim to observe dynamics of the probability of the ground state, $P(t_f)$, for specified values of g_{min} and coupling strength, g^2 within the range of validity, while varying the inverse temperature, β and final runtime, t_f. As follows from figure 4.1 and figure 4.2(c), we can see that at really low coupling strengths, the probability of ground state at the end of runtime, t_f is largely unaffected due to temperature effects in the given simple decay model equation (4.12). However, with increase in coupling strength within the validity regime, figure 4.2(a) and figure 4.2(b), we can observe the temperature effects clearly. While for lower temperatures, the system continues to provide high $P(t_f)$, with higher temperatures and longer runtimes, the value of $P(t_f)$ starts decreasing. For higher temperatures, the shorter runtime provide better $P(t_f)$. The temperature effects become stronger with decrease in g_{min} or conversely, the increase in system size. Recalling [15], the minimum energy gap g_{min} is inversely proportional to square root of the number of basis states which depend upon the number of qubits.

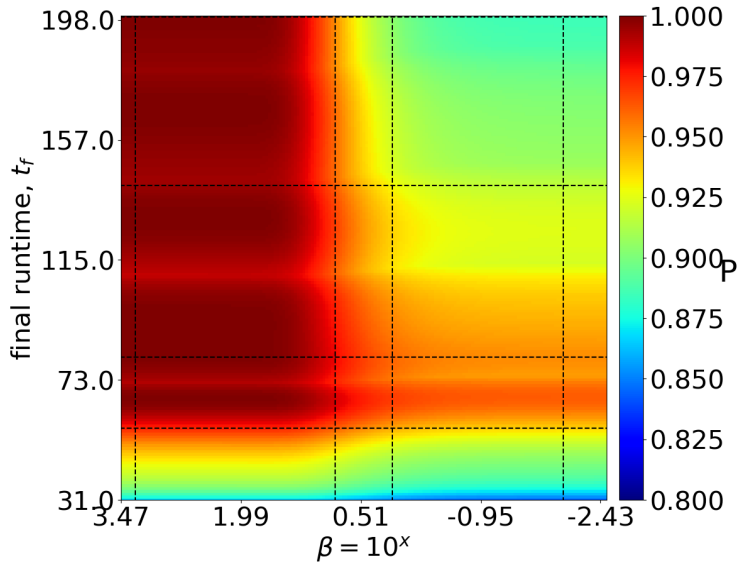

(a) $g^2 = 0.01, g_{min} = 0.1, \beta\, vs\, t_f$

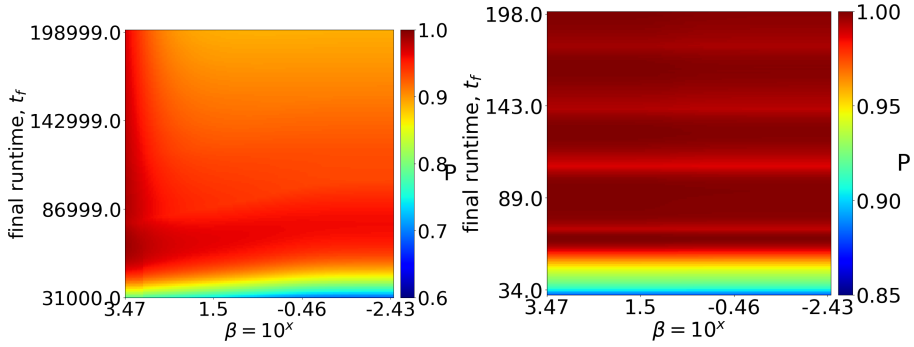

(b) $g^2 = 0.01, g_{min} = 0.0001, \beta\, vs\, t_f$ (c) $g^2 = 0.0001, g_{min} = 0.1, \beta\, vs\, t_f$

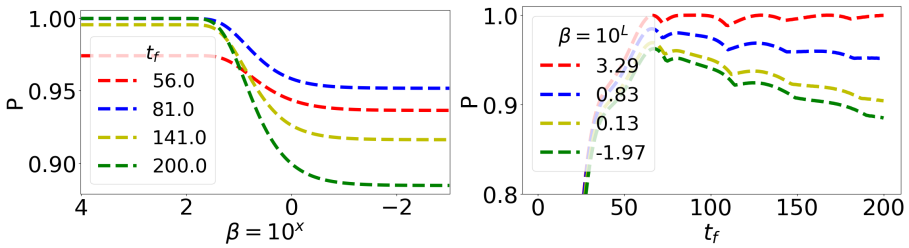

(d) $g^2 = 0.01, g_{min} = 0.1, \beta\, vs\, P$ (e) $g^2 = 0.01, g_{min} = 0.1, t_f\, vs\, P$

Figure 4.2: Plotting probability, $P(t_f)$ of being in instantaneous ground state of the AQC search Hamiltonian in computational basis while varying inverse temperature, β vs final runtime, t_f for specified values of coupling strength, g^2 and minimum energy gap, g_{min}. Note the colour scales for T are different in each sub-figure. The 2-d slice plots (d) and (e) provide a clearer picture of the variation of $P(t_f)$ at different values of the parameters. The single avoided crossing model describing a two-level approximation of multi-qubit AQC search in presence of an ohmic bath is being analysed. The plots provide an outlook on the variation of $P(t_f)$ with temperature under specified values of other parameters.

These effects are exhibited better in figures 4.2(d) and 4.2(e), which are horizontal and vertical slices for specified values of final runtime, t_f and inverse temperature, β in figure 4.2(a). Finally, we will be observing the dynamics of probability of the ground state at the end of runtime, $P(t_f)$ while varying the minimum energy gap, g_{min} or conversely the system size and the inverse temperature, β to observe their correlations for specified values of coupling strength, g^2 and the appropriately chosen t_f for the associated g_{min} values.

A common feature observed in all the plots of figure 4.3 is the loss in value of probability of ground state at the end of runtime, $P(t_f)$ with increase in temperature no matter what the system size may be. While we observe for smaller system size that, $P(t_f)$ is close to 1 low temperatures and loss in value occurs at approaching intermediate and high temperatures, for larger system size, we observe that the loss in value of probability occurs even at low temperatures. The point where the loss in value of $P(t_f)$ starts occurring seems to be linearly decreasing with decrease in g_{min} and increase in β or decrease in temperature. These effects are better exhibited in figures 4.3(d) and 4.3(e), which are horizontal and vertical slices of figure 4.3(a) for specified values of inverse temperature, β and minimum energy gap, g_{min}. We observe in figure 4.3(c) that, while with lower coupling strength the loss of value in $P(t_f)$ is much lower, the point where loss of value in $P(t_f)$ occurs seems to be linearly related in the same manner. Similarly, in figure 4.3(b), we observe that while the region of high probability is more spread out with relatively lower $P(t_f)$, the point where loss of value in $P(t_f)$ occurs is still linearly correlated. Another peculiar feature to be observed is that, figure 4.3(a) and 4.3(c),while there is a dip in $P(t_f)$ at higher temperatures for a particular range of relatively higher coupling strengths for longer runtime chosen, in figure 4.3(b) with shorter runtimes, there is peaking behaviour in $P(t_f)$ instead of a dip. We are not sure whether this is a nuance of the numerics of this particular model, or a general feature in performance of this class of algorithms.

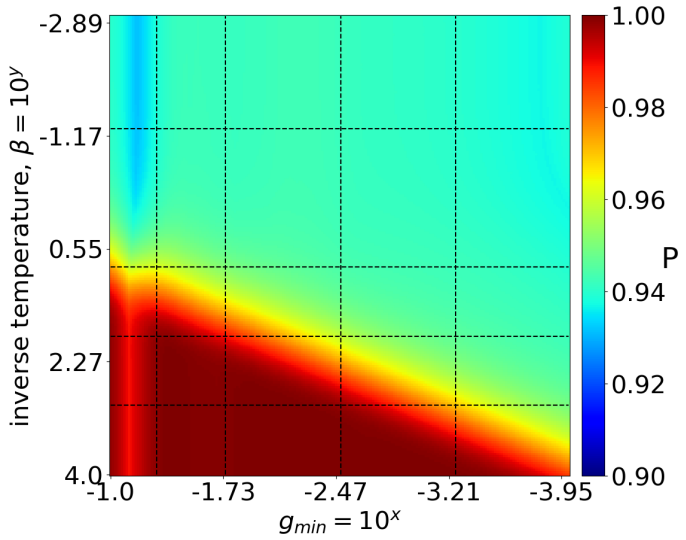

(a) $g^2 = 0.01, t_f = \frac{10}{g_{min}}, g_{min}\, vs\, \beta$

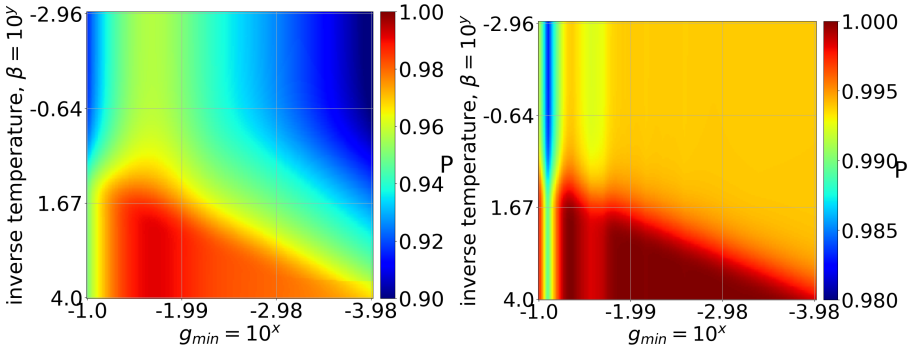

(b) $g^2 = 0.01, t_f = \frac{5}{g_{min}}, g_{min}\, vs\, \beta$ (c) $g^2 = 0.001, t_f = \frac{10}{g_{min}}, g_{min}\, vs\, \beta$

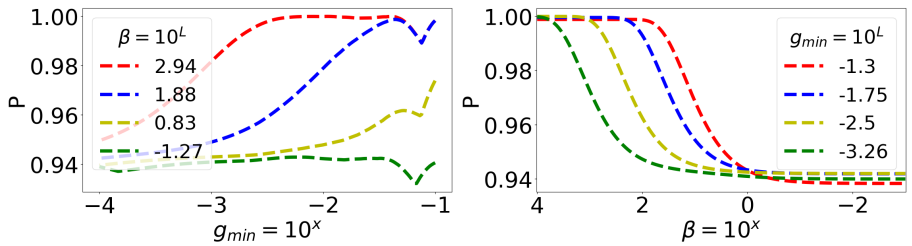

(d) $g^2 = 0.01, t_f = \frac{10}{g_{min}}, g_{min}\, vs\, P$ (e) $g^2 = 0.01, t_f = \frac{10}{g_{min}}, \beta\, vs\, P$

Figure 4.3: Plotting probability, $P(t_f)$ of being in instantaneous ground state of AQC search Hamiltonian in computational basis while varying minimum energy gap, g_{min} vs inverse temperature, β for specified values of coupling strength, g^2 and final runtime, t_f. Note the colour scales for P are different in each sub-figure. The 2-d slice plots (d) and (e) provide a clearer picture of the variation of $P(t_f)$ at different values of the parameters. The single avoided crossing model describing a two-level approximation of multi-qubit AQC search in presence of an ohmic bath is being analysed. The plots provide an outlook on the variation of $P(t_f)$ under different temperatures and system sizes with specified values of other parameters. They show that under specific operating ranges of parameters, the values of $P(t_f)$ is more robust under temperature effects.

Chapter 5

Conclusions

We used a single avoided crossing model to describe a two-level approximation of the quantum walk and AQC search algorithm. The two-level approximation can be used for number of qubits, $n > 7$ since the minimum energy gap $\min(\varepsilon_1(t) - \varepsilon_0(t))$ decreases exponentially faster with system size compared to $\min(\varepsilon_2(t) - \varepsilon_0(t))$ and after $n > 7$ the approximation becomes more and more accurate with increasing system size [22]. The minimum energy gap used in this work range from 10^{-1} to 10^{-4}, which approximately describes the range of number of qubits from $n = 7$ to $n = 27$. The inverse temperature, β is equivalent to $\frac{1}{k_b T}$. We consider $\beta < 1$ to be high temperature, $1 < \beta < 10$ is considered intermediate temperature, $\beta > 10$ is considered low temperature. While coupling strength controls the strength of decoherence and hence affects the success probability of the algorithm, the general behaviour of the model is dependent on β and the minimum gap, g_{min}. It is to be noted that this particular dependence is for the performance of search algorithm in presence of an ohmic bath, the performance of other quantum algorithms in presence of other bath systems could be different with different relevant operating ranges.

For a single avoided crossing model describing a two-level approximation of multi-qubit quantum walk search algorithm in presence of an ohmic bath, we observe within the validity regime of the model that performance of the algorithm worsens

with increase in coupling strength and the size of the system (decreasing g_{min}) due to decoherence and Lamb shift effects. While the best performance is observed at low temperatures with performance being significantly worse at high temperature, there are peculiar effects observed at low temperature where an optimal low temperature for the performance was observed for a specific system size and coupling strength. I believe there will be more interesting features to be observed where temperature can be used for advantage in multi-level models and more realistic thermal bath models.

For a single avoided crossing model describing a two-level approximation of multi-qubit adiabatic quantum computation search algorithm in presence of an ohmic bath, we observe within the validity regime of the model that performance of the algorithm generally worsens with increase in temperature at relatively stronger coupling strengths. For higher temperatures, shorter runtimes provided better performance. Peculiar effects have been observed for correlated ranges of system sizes and coupling strength that at particular range of runtimes, the system performance is less affected by the increase in temperature. There can be valuable further research in this effect, it will be useful to find out operating parameters for a computing system where temperature effects can be reduced even at relatively stronger coupling.

Given a fixed temperature and system bath-coupling, what method is more suitable AQC or quantum walk for performing a search algorithm? The answer to this question is tricky, since they describe different types of system and involves many other factors affecting this choice. The quantum walk in this work describes a time independent process which can be run repeatedly and continuously for long time whereas the AQC describes a time dependent slow changing process with a finite runtime. Considering that the process a system is made to undergo is matter of choice. Quantum walk is more feasible to be used at relatively stronger system-bath coupling and higher temperature since they can provide solutions even in presence of decoherence whereas AQC doesn't provide a reliable solution. However at lower

temperatures AQC is more reliable even for relatively stronger coupling strengths and provide a stable solution. At intermediate temperature, a combination of system size, coupling strength and performance requirements have to be considered to make an informed choice. It is to be noted that with increasing system size, the system bath coupling strength has to still follow the weak coupling approximation for the given model to be valid.

The justification for using a single bath for the single avoided crossing model to draw conclusions about many qubits coupled to identical local baths is beyond the scope of the project but will appear in the paper in preparation.

Bibliography

[1] Salvador E. Venegas-Andraca, *Quantum walks: a comprehensive review*, 2012. Quantum Information Processing. 11 (5): 1015–1106. doi:10.1007/s11128-012-0432-5; arXiv:1201.4780

[2] Viv Kendon, *Decoherence in Quantum walks- a review*, 2006. Math. Struct. in Comp. Sci 17(6) pp 1169-1220 (2006). doi: 10.1017/S0960129507006354; arXiv:quant-ph/0606016v3

[3] T. Kadowaki, H. Nishimori, *Quantum annealing in the transverse Ising model*, 1998. Physical Review E. 58 (5): 5355 (1998). doi: 10.1103/PhysRevE.58.5355; arXiv:cond-mat/9804280

[4] E. Farhi, J. Goldstone, S. Gutmann, and M. Sipser,*Quantum computation by adiabatic evolution*, 2000. arXiv: quant-ph/0001106

[5] Andris Ambainis, *Quantum walks and their algorithmic applications*, 2003. International Journal of Quantum Information. 1 (4): 507–518. doi: 10.1142/S0219749903000383; arXiv:quant-ph/0403120

[6] T.F. Ronnow, Z. Wang, J. Job,S. Boixo, S.V. Isakov, D. Wecker, J.M. Martinis, D.A. Lidar, M. Troyer, *Defining and detecting quantum speedup*, 2014. Science. 345 (6195): 420–424. Bibcode:2014Sci...345..420R. doi:10.1126/science.1252319; PMID 25061205 ; arXiv:1401.2910

[7] Miklos Santha. *Quantum walk based search algorithms*, 2008. Theory and Applications of Models of Computation (TAMC), Xian, April, LNCS 4978. 5 (8): 31–46. Bibcode:2008arXiv0808.0059S; arXiv:0808.0059

[8] Peter W. Shor, *Scheme for reducing decoherence in quantum computer memory*, 1995. Phys. Rev. A 52, R2493(R). doi: 10.1103/PhysRevA.52.R2493

[9] Daniel Lidar and Todd Brun, ed. *Quantum Error Correction*, 2013. Cambridge University Press

[10] Toby S. Cubitt, Ashley Montanaro, and Stephen Piddock, *Universal quantum Hamiltonians*, 2018. doi: 10.1073/pnas.1804949115

[11] R.P. Feynman, R.B. Leighton, M. Sands, 1964. *Feynman Lectures on Physics*. Addison Wesley.

[12] E. Farhi, S. Gutmann, *Quantum computation and decison trees*, 1998. Phys. Rev. A58, 915–928. doi: 10.1103/PhysRevA.58.915; arXiv:quant-ph/9706062

[13] A.M. Childs, R. Cleve, E. Deotto, E. Farhi, S. Gutmann, D.A. Spielman, *Exponential algorithmic speedup by a quantum walk*, 2003. In: Proc. 35th Annual ACM STOC. ACM, NY, pp. 59–68. doi: 10.1145/780542.780552; arXiv:quant-ph/0209131

[14] Andrew M. Childs, *Universal computation by quantum walk*, 2008. Phys. Rev. Lett. 102, 180501 (2009), doi: 10.1103/PhysRevLett.102.180501; arXiv:0806.1972 [quant-ph]

[15] Jeremie Roland, Nicolas J. Cerf, *Quantum search by local adiabatic evolution*, 2002. Phys. Rev. A 65, 042308(2002). doi: 10.1103/PhysRevA.65.042308; arXiv:quant-ph/0107015

[16] M. Born, V. Fock, *Beweis des adiabatensatzes*, 1928. Z.Phys. 51(3-4), 165-180 (1928). doi: 10.1007/BF01343193

[17] Tameem Albash, Daniel A. Lidar, *Adiabatic quantum computing*, 2016. Rev. Mod. Phys. 90, 015002 (2018), doi: 10.1103/RevModPhys.90.015002; arXiv:1611.04471

[18] Dorit Aharonov, Wim van Dam, Julia Kempe, Zeph Landau, Seth LLoyd, *Adiabatic Quantum Computation is Equivalent to Standard Quantum Computation*, 2007. SIAM Journal on Computing. 37: 166. doi:10.1137/s0097539705447323; arXiv:quant-ph/0405098

[19] L.K. Grover, *A fast quantum mechanical algorithm for database search*, 1996. Proceedings, 28th Annual ACM Symposium on the Theory of Computing, (May 1996) p. 212. arXiv:quant-ph/9605043v3

[20] Andrew Childs and Jeffrey Goldstone, *Spatial search by quantum walk*, 2004. Phys. Rev. A 70, 022314 (2004). doi: 10.1103/PhysRevA.70.022314; arXiv:quant-ph/0306054.

[21] A. M. Childs, E. Deotto, E. Farhi, J. Goldstone, S. Gutmann, A. J. Landahl, *Quantum search by measurement*, 2002. Phys. Rev. A 66, 032314 (2002). doi: 10.1103/PhysRevA.66.032314; arXiv:quant-ph/0204013.

[22] J.G. Morley, N. Chancellor, S. Bose, Viv Kendon, *Quantum search with hybrid adiabatic-quantum walk algorithms and realistic noise*, 2019, Phys. Rev. A 99, 022339 (2019), doi: 10.1103/PhysRevA.99.022339 arXiv:1709.00371v3

[23] S. Chakraborty, L. Novo, A. Ambainis, Y. Omar, *Spatial search by quantum walk is optimal for almost all graphs*, 2016. Physical Review Letters 116, 100501 (2016). doi: 10.1103/PhysRevLett.116.100501; arXiv:1508.01327v3 [quant-ph]

[24] Tameem Albash, Daniel A. Lidar, *Decoherence in adiabatic quantum computation*, 2015. arXiv:1503.08767v2

[25] Tameem Albash, Sergio Boixo, Daniel A. Lidar, Paolo Zanardi, *Quantum Adiabatic Markovian Master Equations*, 2015. Phys. Rev. A 91, 062320 (2015). doi: 10.1103/PhysRevA.91.062320; arXiv:1206.4197v5

Appendix A

Analytical expansion of Lamb shift terms for QW search

The analytical calculations for Lamb shift terms, involves solving for integrals containing Cauchy principal value, this makes the calculations fairly complicated. We used the contour integral approach to gain these results in Mathematica software,

$$S(\omega_x) = \frac{1}{1+\omega_x^2} e^{-\beta\omega_x} g^2 \Bigg[-\pi i\omega_x - \frac{\pi}{2}(1+\cos(\beta))\cosh(\beta\omega_x) + \omega_x expintegralei(\beta\omega_x)$$

$$-\frac{\pi}{2}(1+\cos(\beta))\sinh(\beta\omega_x) + e^{\beta\omega_x}[\omega_x log(\omega_x) - cosintegral(\beta)[\omega_x\cos(\beta)+\sin(\beta)]$$

$$+\frac{\pi}{2}\omega_x\sin(\beta) + (\cos(\beta) - \omega_x\sin(\beta))sinintegral(\beta)]\Bigg],$$

$$S(-\omega_x) = \frac{1}{1+\omega_x^2} e^{-i\beta} g^2 \Bigg[e^{\beta(i+\omega_x)}\omega_x\Gamma[0,\beta\omega_x] + [\cos(\beta)+i\sin(\beta)][-\frac{\pi}{2}(1+\cos(\beta)) - \omega_x log(\omega_x)$$

$$+cosintegral(\beta)[\omega_x\cos(\beta)-\sin(\beta)] - \frac{\pi}{2}\omega_x\sin(\beta) + (\cos(\beta)+\omega_x\sin(\omega_x))sinintegral(\beta)]\Bigg].$$

Appendix B

Components of density matrix in solution of AQC search

The rest of the equations for the computational basis density matrix components are:

$$\frac{d}{dt}\rho_{11}^{(c)}(t) = i\Bigg[\rho_{10}^{(c)}(t) - \rho_{01}^{(c)}(t)][\frac{1}{2}(\lambda_+ + \lambda_-)[S(-\Delta(t)) - S(\Delta(t))] + g_{min}[1 - s(t)]\Bigg]$$

$$+\frac{1}{4}\gamma(\Delta(t))\Bigg[\lambda_+^2\rho_{00}^{(c)}(t) - (\lambda_+ + \lambda_-)[\rho_{01}^{(c)}(t) + \rho_{10}^{(c)}(t)] - \lambda_-^2\rho_{11}^{(c)}(t)\Bigg]$$

$$+\frac{1}{4}\gamma(-\Delta(t))\Bigg[\lambda_-^2\rho_{00}^{(c)}(t) - (\lambda_+ + \lambda_-)[\rho_{01}^{(c)}(t) + \rho_{10}^{(c)}(t)] - \lambda_+^2\rho_{11}^{(c)}(t)\Bigg],$$

$$\frac{d}{dt}\rho_{01}^{(c)}(t) = \frac{d}{dt}\rho_{10}^{*(c)}(t) = i\Bigg[\rho_{01}^{(c)}(t)(1-2s(t))+g_{min}[\rho_{00}^{(c)}(t)-\rho_{11}^{(c)}(t)](1-s(t))+\frac{1}{2}(\lambda_+ + \lambda_-)\rho_{00}^{(c)}(t)$$

$$-\frac{1}{2}(\lambda_+ + \lambda_-)\rho_{11}^{(c)}(t) + (\frac{1}{4}\lambda_-^2 - \frac{3}{4}\lambda_+^2)\rho_{01}^{(c)}(t)\Bigg]$$

$$+\gamma(\Delta(t))\Bigg[(-\frac{1}{4}\lambda_- + \frac{3}{4}\lambda_+)\rho_{00}^{(c)}(t) + (\frac{1}{4}\lambda_- - \frac{3}{4}\lambda_+)\rho_{11}^{(c)}(t) - (2 + \frac{1}{8}\lambda_-^2 + \frac{1}{8}\lambda_+^2)\rho_{01}^{(c)}(t)\Bigg]$$

$$+\gamma(-\Delta(t))\Bigg[(\frac{3}{4}\lambda_- - \frac{1}{4}\lambda_+)\rho_{00}^{(c)}(t) + (-\frac{3}{4}\lambda_- + \frac{1}{4}\lambda_+)\rho_{11}^{(c)}(t) - (2 + \frac{1}{8}\lambda_-^2 + \frac{1}{8}\lambda_+^2)\rho_{01}^{(c)}(t)\Bigg].$$